VOLTAGE CONTROL IN AN HVDC SYSTEM TO SHARE PRIMARY FREQUENCY RESERVES BETWEEN NON-SYNCHRONOUS AREAS

Jing Dai, Yannick Phulpin
Supélec
Gif-sur-Yvette, France
jing.dai@supelec.fr, email@yphulpin.eu

Alain Sarlette, Damien Ernst
University of Liège
Liège, Belgium
alain.sarlette@ulg.ac.be, dernst@ulg.ac.be

Abstract - This paper addresses the problem of frequency control for non-synchronous AC areas connected by a multi-terminal HVDC grid. It proposes a decentralized control scheme for the DC voltages of the HVDC converters aimed to make the AC areas collectively react to power imbalances. A theoretical study shows that, by using local information only, the control scheme allows to significantly reduce the impact of a power imbalance by distributing the associated frequency deviation over all areas. A secondary frequency control strategy that can be combined with this control scheme is also proposed so as to restore the frequencies and the power exchanges to their nominal values in the aftermath of a power imbalance. Simulation results on a benchmark system with five AC areas illustrate the good performance of the control scheme.

Keywords - frequency control, multi-terminal HVDC system, primary frequency reserve

1 Introduction

THIS paper addresses the problem of coordinating frequency control efforts among non-synchronous AC areas connected by a multi-terminal HVDC system. It focuses mainly on short-term control actions, referred to as primary frequency control. A conventional approach is to modify the power injections into the DC grid based on frequency measurements of all areas so as to make their frequency deviations evolve towards the same value, which makes the AC areas collectively react to power imbalances. This type of application is considered in [1] and [2] in the context of a system with two non-synchronous AC areas, and is generalized in [3] to an arbitrary number of AC areas. Since this approach requires transmission of frequency information among the AC areas, considerable delays (of the order of a few seconds [4]) can be involved. As shown in [5], such delays reduce the efficiency of the control scheme and may even lead to instability.

In the present paper, we propose a decentralized control scheme that is based only on local measurements so as to avoid the problems related to the dependence on remote information. More specifically, our new scheme controls every converter based on the frequency of the AC area it is connected to. Additionally, rather than directly controlling the *power injections* into the DC grid, as is done in [1], [2], [3], [5], the new scheme controls the *DC voltages* of the converters.

Theoretical analysis of a simplified case supports that the interconnected system under the new control scheme converges, after a change of load demands in the AC areas, to a unique stable equilibrium with shared frequency deviations. The higher the controller gain, the closer the frequency deviations of the different AC areas stay to each other at this equilibrium point. Simulations on a benchmark system with five AC areas highlight that the control scheme indeed makes the frequency deviations of all areas exhibit the same variation pattern, and, consequently, that the primary frequency reserves are effectively shared among the areas. The simulations also show that the DC voltages of the HVDC converters remain within an acceptable range.

While this control scheme ensures that the primary frequency reserves are indeed shared, the frequencies of the AC areas and the power exchanges between them are different from the nominal values once the system has reached a new equilibrium point. To restore the frequencies and the power exchanges, we propose in the last part of this paper a strategy for adjusting the power settings of the generators. This strategy is largely inspired from the secondary frequency control scheme recommended by the UCTE [4].

The paper is organized as follows. Section 2 describes the multi-terminal HVDC system model used in our study. Section 3 details our control scheme for sharing primary frequency reserves. Section 4 theoretically analyzes the stability of the controlled system. Section 5 presents a benchmark system and simulation results. Section 6 shows how to combine the first control scheme with a secondary frequency control strategy.

2 Multi-terminal HVDC system model

We consider a system with three types of components: a DC grid, N non-synchronous AC areas, and N converters that interface the AC areas with the DC grid, as depicted in Fig. 1. These components are detailed in this section, whose material is largely borrowed from [3].

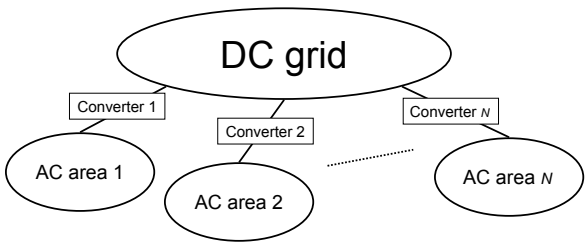

Figure 1: A multi-terminal HVDC system connecting N AC areas via N converters.

2.1 DC grid

As the electrical time constant of a DC grid is of the order of a few tens of milliseconds [6], transient dynamics of the DC grid is not considered.

We suppose that every node in the DC grid is connected to a converter. Each node inherits the index number of the AC area to which it is connected. Then, the power injection from AC area i into the DC grid, denoted by P_i^{dc}, satisfies

$$P_i^{dc} = \sum_{j=1}^{N} \frac{V_i^{dc}(V_i^{dc} - V_j^{dc})}{R_{ij}}\,, \tag{1}$$

where V_i^{dc} and V_j^{dc} are the voltages at nodes i and j, respectively, and R_{ij} is the resistance between these two nodes. V_i^{dc} is called the DC-side voltage of converter i in the following. Note that $R_{ij} = R_{ji}$. If nodes i and j are not directly connected, R_{ij} is considered equal to infinity. We consider a DC grid in which there is either a direct or an indirect connection between any two nodes, such that it is not made of several isolated parts.

Under normal operation conditions, a very small voltage difference between two nodes corresponds to a significant power flow. Therefore, $V_1^{dc}, \ldots, V_N^{dc}$ are close to the rated voltage of the HVDC system, denoted by V_{ref}^{dc}.

2.2 Converters

We neglect the high-frequency characteristics of the converters, for the same reason as the DC transients. We assume that a converter can track instantaneously a reference signal for either the power injection into the DC grid via the converter P_i^{dc} or the converter's DC-side voltage V_i^{dc}.

2.3 AC areas

On the time scale of primary frequency control, the frequency can be considered identical in any part of an AC area. We use therefore an aggregated model to represent the loads and the generators within each area.

The sum of the loads within area i, denoted by P_{li}, is represented by a static load model [7]

$$P_{li} = P_{li}^o \cdot (1 + D_{li}(f_i - f_{nom,i}))\,, \tag{2}$$

where f_i is the frequency of area i, $f_{nom,i}$ is its nominal value, P_{li}^o is the power drawn by the load when $f_i = f_{nom,i}$, and D_{li} is the frequency sensitivity factor.

The mechanical dynamics of the generator for area i is described by the equation of motion

$$2\pi J_i \frac{df_i}{dt} = \frac{P_{mi} - P_{li} - P_i^{dc}}{2\pi f_i} - 2\pi D_{gi}(f_i - f_{nom,i})\,, \tag{3}$$

where P_{mi}, J_i, and D_{gi} are respectively the mechanical power input, the moment of inertia, and the damping factor of the aggregated generator for area i. These parameters can be obtained by aggregation methods as in [8].

We assume that every AC area has the same type of primary frequency control, where the aggregated generator is equipped with a speed governor that observes the rotating speed of the shaft and adjusts P_{mi} accordingly, following

$$T_{smi}\frac{dP_{mi}}{dt} = P_{mi}^o - P_{mi} - \frac{P_{nom,i}}{\sigma_i}\frac{f_i - f_{nom,i}}{f_{nom,i}}\,, \tag{4}$$

where σ_i is the generator droop, T_{smi} the time constant of the servomotor, $P_{nom,i}$ the rated mechanical power of the generator, and P_{mi}^o the setting value for P_{mi}.

The variations of P_{mi} are bounded by some technical and economical constraints. Formally, we suppose that for the generator of area i, the constraints can be expressed by

$$P_{mi}^{\min} \le P_{mi} \le P_{mi}^{\max}\,, \tag{5}$$

where $P_{mi}^{\max}$ and $P_{mi}^{\min}$ are the maximum and the minimum power that can be produced by generator i. The difference between $P_{mi}^{\max}$ and P_{mi}^o is referred to as primary frequency reserve. As the primary frequency reserves are an expensive industrial resource [9], we aim to introduce a control scheme which allows to effectively share them among different AC areas.

3 HVDC frequency control scheme

In this section, we first define the equilibrium point at which the system is assumed to be prior to any disturbance and which will be called later the reference operating point. Then, we describe a control scheme that adjusts converters' DC voltages to allow primary frequency reserve sharing.

3.1 Reference operating point

The reference operating point of the system is a steady state defined by specific values of the input parameters (P_{li}^o, P_{mi}^o) and of the variables (f_i, P_{mi}, P_{li}, P_i^{dc}, V_i^{dc}). In the following, we denote by $\bar{P}_{li}^o$ and $\bar{P}_{mi}^o$ the values of P_{li}^o and P_{mi}^o at the reference operating point, respectively. We also denote the values of the variables at this point by their corresponding symbols with a bar overhead.

We take the frequencies at the reference operating point equal to their nominal values, i.e.

$$\bar{f}_i = f_{nom,i}\,, \quad \forall i \in \{1, \ldots, N\}\,. \tag{6}$$

Then, (2) directly yields,

$$\bar{P}_{li} = \bar{P}_{li}^o\,, \quad \forall i \in \{1, \ldots, N\}\,. \tag{7}$$

Since this reference operating point is an equilibrium point of each area, we get from (3) and (4)

$$\bar{P}_{mi} = \bar{P}_{mi}^o\,, \qquad \forall i \in \{1, \ldots, N\}\,, \tag{8}$$

$$\bar{P}_i^{dc} = \bar{P}_{mi}^o - \bar{P}_{li}^o\,, \qquad \forall i \in \{1, \ldots, N\}\,. \tag{9}$$

The DC load flow equation (1) provides a final set of equations linking the voltage values to the other variables

$$\bar{P}_i^{dc} = \sum_{j=1}^{N} \frac{\bar{V}_i^{dc}(\bar{V}_i^{dc} - \bar{V}_j^{dc})}{R_{ij}}\,, \quad \forall i \in \{1, \ldots, N\}\,. \tag{10}$$

In practice, the values of power inputs $\bar{P}^o_{mi}$ are chosen such that, for reference loads and nominal frequencies, Equations (9) and (10) have a unique solution with one of the voltages $\bar{V}^{dc}_i$ equal to V^{dc}_{ref}.

3.2 Control scheme

Sharing primary frequency reserves between AC areas means that any area subjected to a power imbalance can rely on the reserves provided not only by local generation but also by generators located in other areas. As frequency control usually relies on frequency measurements, which reflect the power balance of a synchronous area, a conventional way to achieve the above objective is to emulate a large AC interconnection so that the frequency deviations of all areas remain equal at all times.

In this paper, we propose a control scheme that makes - as we will show later - the frequency deviations of all the areas stay arbitrarily close to each other. This scheme is decentralized in nature and it is composed of N subcontrollers, one for each HVDC converter. More specifically, subcontroller i modifies the DC-side voltage of converter i such that

$$V^{dc}_i = \bar{V}^{dc}_i + \alpha_i (f_i - \bar{f}_i)\,, \tag{11}$$

where $\alpha_i \geq 0$ is the gain of subcontroller i.

The intuition behind the control law is as follows. If for instance area i has more generation than the sum of the load and the injection into the DC grid, then its frequency f_i will increase. To restore the balance of area i, more power should be injected from area i into the DC grid. To achieve this, the DC voltage V^{dc}_i is increased so that the voltage difference $V^{dc}_i - V^{dc}_j$ becomes higher, under unchanged V^{dc}_j, for all $j \neq i$. By virtue of (1), this yields increased power exchanges from area i to the other areas. The other areas, injecting less power into (or equivalently, getting more power from) the DC grid, see their frequencies increase and as a consequence also raise their voltages. In conclusion, the network as a whole reacts to the imbalance in area i, distributing the voltage and the frequency deviation over the whole network.

The value of subcontroller gain α_i has a significant impact on the dynamics of the system. Roughly speaking, an area with a larger value of α_i will stay closer to its nominal frequency than an area with a smaller α_i. For simplicity, we assume in the following that all the subcontrollers have the same gain, denoted by α.

3.3 Constraints

To ensure normal operation of the HVDC system, the control variables should be modulated subject to

$$V^{dc,\min}_i \leq V^{dc}_i \leq V^{dc,\max}_i, \quad \forall i \in \{1,\dots,N\}\,, \tag{12}$$

where $V^{dc,\min}_i$ and $V^{dc,\max}_i$ are the minimum and the maximum acceptable values of V^{dc}_i. In practice, these values depend on both the technological characteristics of converter i and the DC voltages of the other converters in the DC grid. Indeed, appropriate $V^{dc,\min}_i$ and $V^{dc,\max}_i$ are meant to ensure that the transmission limits of the DC lines and the power ratings of the converters are not exceeded.

4 Stability analysis

This section studies the stability of the system around the reference operating point. We focus on small variations of the load, and consider thus a linearized system. We first prove the existence of a unique equilibrium point. Second, for the particular case where all AC areas have identical parameters, we prove stability using a frequency-domain approach. Afterwards, the unique equilibrium point for this case is characterized to highlight the effectiveness of the controller and illustrate the influence of the controller gain.

Let us linearize the system around the reference operating point. The nonlinear equation resulting from (2) and (3) is linearized around the reference operating point as

$$2\pi J_i \frac{df_i}{dt} = \frac{P_{mi} - P^o_{li} - P^{dc}_i}{2\pi f_{nom,i}} - 2\pi D_i (f_i - f_{nom,i})\,, \tag{13}$$

where $D_i = D_{gi} + \bar{P}^o_{li} D_{li}/(4\pi^2 f_{nom,i})$.

As all V^{dc}_i are usually close to V^{dc}_{ref}, we approximate (1) by

$$P^{dc}_i = \sum_{j=1}^{N} \frac{V^{dc}_{ref}(V^{dc}_i - V^{dc}_j)}{R_{ij}}\,. \tag{14}$$

The theoretical analysis in this section focuses on the system characterized by Equations (4), (11), (13), (14) for all $i \in \{1,\dots,N\}$.

We denote by $\mathbf{0}_N$ (resp. $\mathbf{1}_N$) the column-vector of length N with all its elements equal to 0 (resp. to 1).

4.1 Equilibrium point

Proposition 1. *Given fixed mechanical power setting $P^o_{mi} = \bar{P}^o_{mi}$, the (linearized) system defined by* (4), (11), (13), (14) *for all $i \in \{1,\dots,N\}$ has a unique equilibrium point for any load demand value P^o_{li}.*

Proof. We introduce the following variables: $x_i = f_i - \bar{f}_i$, $y_i = P_{mi} - \bar{P}_{mi}$, $z_i = V^{dc}_i - \bar{V}^{dc}_i$, $u_i = P^{dc}_i - \bar{P}^{dc}_i$ and, for the load demand input, $v_i = P^o_{li} - \bar{P}^o_{li}$. With these variables and taking (6)-(10) into account, the equilibrium conditions associated to (4), (11), (13), (14) become

$$y_i = -c_{1i} x_i\,, \tag{15}$$

$$z_i = \alpha x_i\,, \tag{16}$$

$$y_i = u_i + v_i + c_{2i} x_i\,, \tag{17}$$

$$u_i = \sum_{j=1}^{N} b_{ij}(z_i - z_j) + b_i\,, \tag{18}$$

where $c_{1i} = P_{nom,i}/(\sigma_i f_{nom,i})$, $c_{2i} = 4\pi^2 f_{nom,i} D_i$, $b_i = \sum_j (V^{dc}_{ref} - \bar{V}^{dc}_i)(\bar{V}^{dc}_i - \bar{V}^{dc}_j)/R_{ij}$ and $b_{ij} = V^{dc}_{ref}/R_{ij}$. Define the column-vectors $\mathbf{x} = [x_1,\dots,x_N]^T$, $\mathbf{y} = [y_1,\dots,y_N]^T$, $\mathbf{u} = [u_1,\dots,u_N]^T$, $\mathbf{v} =$

$[v_1, \ldots, v_N]^T$, $\mathbf{b} = [b_1, \ldots, b_N]^T$, as well as the matrices $C_i = \text{diag}(c_{i1}, \ldots, c_{iN})$, $i = 1, 2$, and L with[1]

$$[L]_{ij} = \begin{cases} -b_{ij} & \text{for } i \neq j\,, \\ \sum_{j \neq i} b_{ij} & \text{for } i = j\,. \end{cases} \tag{19}$$

With these notations, introducing (15), (16), (18) in (17) yields

$$(C_1 + C_2 + \alpha L)\mathbf{x} = -(\mathbf{v} + \mathbf{b})\,. \tag{20}$$

Since c_{1i} and c_{2i} are all strictly positive and L is positive semidefinite, $(C_1 + C_2 + \alpha L)$ is invertible. So a fixed value $\mathbf{v} = \mathbf{v}^e$ defines a single equilibrium value of $\mathbf{x}$

$$\mathbf{x}^e = -(C_1 + C_2 + \alpha L)^{-1}(\mathbf{v}^e + \mathbf{b})\,. \tag{21}$$

From (15), (16), (18) we then readily obtain the equilibrium values of the other vectors

$$\mathbf{y}^e = -C_1\mathbf{x}^e\,, \tag{22}$$

$$\mathbf{z}^e = \alpha\mathbf{x}^e\,, \tag{23}$$

$$\mathbf{u}^e = \alpha L\mathbf{x}^e + \mathbf{b}\,. \tag{24}$$

□

The equilibrium point defined by (21), (22), (23), (24) for $\mathbf{v}^e = \mathbf{0}_N$ differs from the reference operating point by a term of order $\mathbf{b}$, due to approximation (14). If the latter is valid to first order, then $\mathbf{b}$ is a second-order perturbation that can be neglected.

4.2 Stability of the system with identical AC areas

Theoretically proving stability of the system for the general case is particularly difficult. We present hereafter a result for the particular case where all AC areas are identical. More precisely, we assume that all system parameters, as well as the nominal frequencies $f_{nom,i}$ and loads $\bar{P}^o_{li}$, are independent of area index i; however, $\bar{P}^o_{mi}$, $\bar{V}^{dc}_i$ and $\bar{P}^{dc}_i$ can be different from one AC area to the other. Proposition 2 establishes stability of the linearized system. The original, nonlinear system inherits the stability properties of its linearized counterpart provided that $(P^o_{li} - \bar{P}^o_{li})$ and $(\bar{V}^{dc}_i - V^{dc}_{ref})$, i.e. load perturbations and voltage spreadings around reference, are sufficiently small.

Proposition 2. *Suppose that all AC areas of the HVDC system have identical parameters. Given fixed mechanical power setting $P^o_{mi} = \bar{P}^o_{mi}$, consider the (linearized) system with the controller, defined by* (4), (11), (13), (14) *for all $i \in \{1, \ldots, N\}$, with P^o_{li} considered as input. This system is asymptotically stable such that, for any fixed value of P^o_{li}, it converges to the unique equilibrium given by* (21), (22), (23), (24)*.*

Proof. We drop AC area index i when referring to the parameters of the areas that have the same values. With the notations of the proof of Proposition 1, and Equations (21) to (24), the linear system becomes

$$\frac{d\mathbf{x}}{dt} = (A_1 + \alpha' L)(\mathbf{x} - \mathbf{x}^e) + A_2(\mathbf{y} - \mathbf{y}^e) + B(\mathbf{v} - \mathbf{v}^e)\,, \tag{25}$$

$$\frac{d\mathbf{y}}{dt} = A_3(\mathbf{x} - \mathbf{x}^e) + A_4(\mathbf{y} - \mathbf{y}^e)\,, \tag{26}$$

where $A_i = a_i I_N$ with I_N the identity matrix and $a_1 = -D/J$, $a_2 = 1/(4\pi^2 f_{nom} J)$, $a_3 = -c_1/T_{sm}$, and $a_4 = -1/T_{sm}$; also $\alpha' = -\alpha/(4\pi^2 f_{nom} J)$ and $B = -A_2$.

Linear system (25), (26) is asymptotically stable, such that $(\mathbf{x}, \mathbf{y})$ converges to $(\mathbf{x}^e, \mathbf{y}^e)$ when $\mathbf{v} = \mathbf{v}^e$ constant, if and only if the $2N \times 2N$ matrix

$$\mathcal{A} := \begin{pmatrix} A_1 + \alpha' L & A_2 \\ A_3 & A_4 \end{pmatrix} \tag{27}$$

has all its eigenvalues negative. Define $L = VDV^T$ with V orthogonal and D diagonal, containing the eigenvalues λ_i of L which are all strictly positive except $\lambda_1 = 0$. As all A_i are multiples of identity, the matrices $V^T A_i V$ and $V^T L V$ are all diagonal. Then a standard parallel reordering of rows and columns transforms $\mathcal{A}$ into $\widetilde{\mathcal{A}}$ a block-diagonal matrix with the same eigenvalues; the blocks of $\widetilde{\mathcal{A}}$ are of the form

$$Z_i := \begin{pmatrix} a_1 + \alpha'\lambda_i & a_2 \\ a_3 & a_4 \end{pmatrix} \tag{28}$$

for $i = 1, \ldots, N$. From the signs of $\{a_1, \ldots, a_4\}$, α' and λ_i for $i = 1, \ldots, N$, we get that each Z_i has a negative trace and a positive determinant, such that the eigenvalues must all be negative. □

4.3 Characterization of the equilibrium point

The above analysis proves the stability of the system. The present subsection focuses on the objective of the control scheme, i.e. to make the frequency deviations of the different AC areas stay close to each other. For simplicity, the theoretical analysis focuses on the particular case where all AC areas have identical parameters, like for the stability analysis.

Proposition 3. *Suppose that all AC areas of the HVDC system have identical parameters. For any given values of $\bar{V}^{dc}_1, \ldots, \bar{V}^{dc}_N$ and of load demand variation, the difference between the frequencies of the AC areas at the equilibrium point of the (linearized) system can be made arbitrarily small by taking controller gain α sufficiently large.*

Proof. We use hereafter the notations introduced in the proof of Proposition 1.

To measure the differences between $x^e_1, \ldots, x^e_N$, we define $\Delta x^e_i = x^e_i - \bar{x}^e$, where $\bar{x}^e = \frac{1}{N}\sum_{i=1}^N x^e_i$. Let $\Delta\mathbf{x}^e = [\Delta x^e_1, \ldots, \Delta x^e_N]^T$. Let $\mathbf{w}^e = \mathbf{v}^e + \mathbf{b}$ and define $\bar{w}^e$ and $\Delta\mathbf{w}^e$ similarly. We want to bound the Euclidean norm $\|\Delta\mathbf{x}^e\|$ of $\Delta\mathbf{x}^e$.

Let $a = c_1 + c_2$. Then, (20) becomes

$$-\mathbf{w}^e = (\alpha L + aI_N)\mathbf{x}^e\,. \tag{29}$$

[1] In graph theory, L is well-known as the Laplacian matrix associated to an undirected weighted graph. It is symmetric positive semidefinite, with the number of 0 eigenvalues equal to the number of connected components, which here is just one as the whole DC grid is assumed to be connected.

Premultiplying the above equation by $\mathbf{1}_N^T$ yields

$$-\mathbf{1}_N^T \mathbf{w}^e = \mathbf{1}_N^T(\alpha L + aI_N)\mathbf{x}^e = \alpha \mathbf{1}_N^T L \mathbf{x}^e + a\mathbf{1}_N^T \mathbf{x}^e \,. \tag{30}$$

Since $\mathbf{1}_N^T L = \mathbf{0}_N^T$, $\mathbf{1}_N^T \mathbf{x}^e = N\bar{x}^e$, and $\mathbf{1}_N^T \mathbf{w}^e = N\bar{w}^e$, the above equation becomes

$$-\bar{w}^e = a\bar{x}^e \,. \tag{31}$$

On the other hand, (29) can be written as

$$\begin{aligned} & -(\Delta \mathbf{w}^e + \bar{w}^e \mathbf{1}_N) \\ = \;& (\alpha L + aI_N)(\Delta \mathbf{x}^e + \bar{x}^e \mathbf{1}_N) \\ = \;& \alpha L \Delta \mathbf{x}^e + \alpha \bar{x}^e L \mathbf{1}_N + a\Delta \mathbf{x}^e + a\bar{x}^e \mathbf{1}_N \\ = \;& \alpha L \Delta \mathbf{x}^e + a\Delta \mathbf{x}^e + a\bar{x}^e \mathbf{1}_N \,, \end{aligned} \tag{32}$$

where we used the fact that $L\mathbf{1}_N = \mathbf{0}_N$. Given (31), the above equation yields

$$-\Delta \mathbf{w}^e = (\alpha L + aI_N)\Delta \mathbf{x}^e \,. \tag{33}$$

Denote by $\{\omega_1, \ldots, \omega_N\}$ an orthonormal set of eigenvectors of L associated to corresponding eigenvalues $\{\lambda_1 \leq \lambda_2 \leq \ldots \leq \lambda_N\}$. Because L is a Laplacian matrix, we have $\lambda_1 = 0$ associated to $\omega_1 = \frac{1}{\sqrt{N}} \mathbf{1}_N$, and because the grid is connected we have $\lambda_2 > 0$.

Denote by $\Delta\tilde{x}_i^e$ the components of vector $\Delta \mathbf{x}^e$ expressed in orthonormal basis $\mathcal{B} = (\omega_1, \ldots, \omega_N)$, and by $\Delta\tilde{w}_i^e$ the components of $\Delta \mathbf{w}^e$ expressed in this same basis. Because of the orthonormal basis $\mathcal{B}$, we have $\|\Delta \mathbf{x}^e\|^2 = \sum_i |\Delta\tilde{x}_i^e|^2$ and $\|\Delta \mathbf{w}^e\|^2 = \sum_i |\Delta\tilde{w}_i^e|^2$. Then we have from (33), for all $i \in \{1, \ldots, N\}$,

$$|\Delta\tilde{w}_i^e| = (\alpha\lambda_i + a)|\Delta\tilde{x}_i^e| \geq (\alpha\lambda_2 + a)|\Delta\tilde{x}_i^e| \,. \tag{34}$$

The property is obvious for $i \geq 2$; for $i = 1$ it holds because by definition $\Delta\tilde{x}_1^e = \omega_1^T \Delta \mathbf{x}^e = \frac{1}{\sqrt{N}} \mathbf{1}_N^T \Delta \mathbf{x}^e = 0$, such that we get $0 \geq 0$. Therefore, (33) yields

$$\|\Delta \mathbf{w}^e\| = \|(\alpha L + aI_N)\Delta \mathbf{x}^e\| \geq (\alpha\lambda_2 + a)\|\Delta \mathbf{x}^e\| \tag{35}$$

such that we have[2]

$$\|\Delta \mathbf{x}^e\| \leq \frac{1}{\alpha\lambda_2 + a}\|\Delta \mathbf{w}^e\| \leq \frac{1}{\alpha\lambda_2 + a}\|\mathbf{w}^e\| \,. \tag{36}$$

For a given value of $\mathbf{w}^e = \mathbf{v}^e + \mathbf{b}$, which is fixed by $\bar{V}_1^{dc}, \ldots, \bar{V}_N^{dc}$ and load demand variations, the right hand side of this inequality can be made arbitrarily small by taking α sufficiently large. □

Note that in the expression of the bound on $\|\Delta \mathbf{x}^e\|$, the controller gain α is multiplied by λ_2, the second-smallest eigenvalue of L. This eigenvalue is an extensively studied object of graph theory, where it is called the algebraic connectivity. In the context of synchronization, it determines the slowest convergence rate of all the subsystems to the consensus value. In our problem, λ_2 is determined by the topology of the DC grid.

5 Simulations

The effectiveness of the proposed control scheme is illustrated hereafter in the context of a five-area system. After introducing the benchmark system, we report and discuss the simulation results.

5.1 Benchmark system

The benchmark system consists of a multi-terminal HVDC system connecting five non-synchronous areas. The topology of the DC network is represented in Fig. 2. The resistances of the DC links are: $R_{12} = 1.39\Omega$, $R_{15} = 4.17\Omega$, $R_{23} = 2.78\Omega$, $R_{25} = 6.95\Omega$, $R_{34} = 2.78\Omega$, and $R_{45} = 2.78\Omega$. In our simulations, we consider that individual AC areas significantly differ from each other, see the parameters in Table 1.

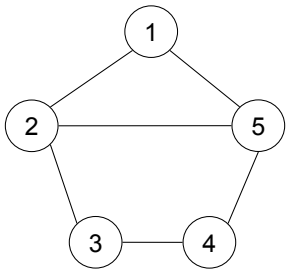

Figure 2: DC grid topology. The circle numbered i represents the point in the DC grid to which converter i is connected. An edge between two circles represents a DC line.

	Area					Unit
	1	2	3	4	5	
f_{nom}	50	50	50	50	50	Hz
P_m^o	50	80	50	30	80	MW
P_{nom}	50	80	50	30	80	MW
J	2026	6485	6078	2432	4863	kg m^2
D_g	48.4	146.3	140.0	54.9	95.1	W s^2
σ	0.02	0.04	0.06	0.04	0.03	
T_{sm}	1.5	2.0	2.5	2	1.8	s
P_l^o	100	60	40	50	40	MW
D_l	0.01	0.01	0.01	0.01	0.01	Hz^{-1}

Table 1: Parameters at the reference operating point of the AC areas.

The system is supposed to operate initially at the reference operating point with $\bar{V}_5^{dc} = V_{ref}^{dc} = 100$kV. At time $t = 2$s, the value of P_{l2}^o jumps from $\bar{P}_{l2}^o = 60$MW to $1.05 \cdot \bar{P}_{l2}^o = 63$MW. We observe the evolution of the system over the next 28 seconds.

The nonlinear model presented in Section 2 is used for the simulations. The continuous-time differential equations (3) and (4) are integrated using the Euler method with a time-discretization step of 1ms.

5.2 Simulation results

Figure 3 depicts the evolution of the frequencies when $\alpha = 2 \times 10^3$. For comparison, it also shows the evolution of f_2 when $\alpha = 0$ (i.e. no control action, $V_1^{dc}, \ldots, V_5^{dc}$ are kept constant). These simulations show that without the controller ($\alpha = 0$), the frequency of area 2 undergoes

[2]The last inequality directly follows by writing $\Delta \mathbf{w}^e = (I_N - \omega_1 \omega_1^T)\mathbf{w}^e$: when expressed in orthonormal basis $\mathcal{B}$, $\Delta \mathbf{w}^e$ and $\mathbf{w}^e$ differ only in the first component, which equals 0 for $\Delta \mathbf{w}^e$.

a deviation with transient maximum of 0.196Hz and stabilizes at 49.927Hz. With the controller defined by (11), the maximum transient deviation of f_2 drops to 0.055Hz, and the frequencies of the five areas exhibit the same variation pattern and finally settle within a band between 49.976Hz and 49.988Hz. The curves representing the evolution of the control variables, $V_1^{dc}, \ldots, V_5^{dc}$, are not included here, because their variations are proportional to the frequency deviation of the corresponding area. We observe that variations in V_i^{dc} remain smaller than the range of initial values $\bar{V}_i^{dc}$, which indicates that such variations do not result in excessively high or low voltages within the DC grid.

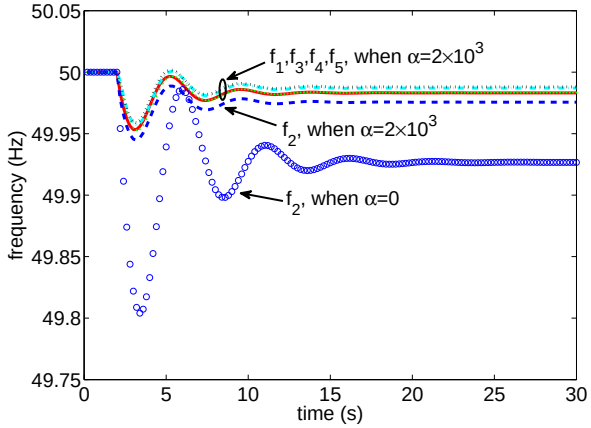

Figure 3: Frequencies of the 5 AC areas after an increase of P_{l2}^o at $t = 2$s, under primary frequency controller (11) only (no secondary frequency control). Dotted lines: f_i for $\alpha = 2 \times 10^3$. Circles: f_2 for $\alpha = 0$ (no control action).

Figure 4 shows the evolution of the power injections from the AC areas into the DC grid, $P_1^{dc}, \ldots, P_5^{dc}$ expressed in MW. Their variations remain within 10% of the original values, which is moderately small.

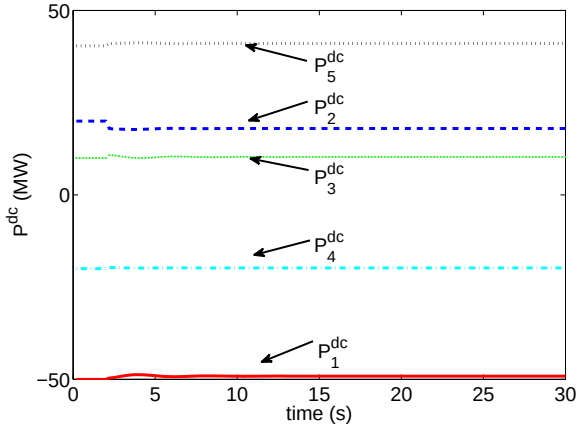

Figure 4: Power injections from the five AC areas into the DC grid.

The above results show that our control scheme leads to a significant improvement in both the steady-state frequency deviations (from 0.073Hz to 0.024Hz) and the maximum transient deviations (from 0.196Hz to 0.055Hz) of area 2. However, the frequency deviations of the different AC areas do not converge to each other and remain within a band, whose width is 0.012Hz. Further simulations show that when α is doubled to 4×10^3, the width of this band is reduced to 0.007 Hz. This indicates that a property similar to Proposition 3 seems to still hold when AC areas have different parameter values.

In the above simulations, we consider the practical case where none of the aggregated generators' primary frequency reserves is depleted. Further simulations show that if the primary frequency reserves of some areas are depleted, i.e. one of the constraints in (5) becomes active, then their frequency deviations will still remain close to each other by exhibiting the same variation patterns, before finally stabilizing within a larger band of the frequency deviations. It is only when *all* areas have their primary frequency reserves depleted that the generators become unable to restore the power balance; thus, in a real power system, emergency control actions such as load-shedding would be triggered by ever-decreasing frequencies only in this extreme case. This shows the efficiency of our controller in sharing primary frequency reserve resources.

6 Coordination with secondary frequency control

The control scheme proposed above makes the AC areas collectively react to power imbalances within the system, but as stated in Proposition 1, the primary frequency control scheme makes neither the frequencies of the AC areas nor the power exchanges between the areas return to their nominal values. To restore the frequencies and the power exchanges, every AC area i must resort to secondary frequency control, which acts on P_{mi}^o, the setting for the mechanical power of the aggregated generator.

To discuss the long-term dynamics of the AC areas connected by an MT-HVDC system under the proposed control scheme, we present in this section one solution for the AC areas to implement secondary frequency control in line with the recommendations of the UCTE.

6.1 Secondary frequency control scheme

Secondary frequency control has two objectives: (i) to restore the frequencies of all the AC areas back to their nominal values; (ii) to restore the power exchanged between control blocks (the AC areas in this paper) back to their scheduled values. These objectives can be achieved if a power imbalance originating in one area i is fully compensated by a change in P_{mi}^o. In a system composed of interconnected areas, it is a real issue to estimate the area of origin and the magnitude of a power imbalance on the basis of available measurements. It can be solved as follows.

In absence of a power imbalance in area i, $(P_{mi}^o - P_{li}^o)$ is a constant value, which implies

$$P_{mi}^o - P_{li}^o = \bar{P}_{mi}^o - \bar{P}_{li}^o = \bar{P}_i^{dc} \,. \tag{37}$$

In this case, the deviations in its power injection P_i^{dc} and frequency f_i induced by any potential imbalances in *other* areas are linked by a linear relation. Indeed, define

$$\delta P_i^{dc} = P_i^{dc*} - (P_{mi}^o - P_{li}^o) = P_i^{dc*} - \bar{P}_i^{dc} \,, \tag{38}$$

$$\delta f_i = f_i^* - f_{nom,i} \,, \tag{39}$$

where values with * indicate equilibrium. Then equations (4) and (13) with equilibrium conditions (time derivatives equal to zero) lead to

$$\delta P_i^{dc} = -\lambda_i^{\text{NPFC}}\, \delta f_i\,, \tag{40}$$

independently of the DC voltages V_j^{dc}, $j = 1,\ldots,N$, with constant $\lambda_i^{\text{NPFC}} = 4\pi^2 f_{nom,i} D_i + P_{nom,i}/(\sigma_i f_{nom,i})$. Parameter λ_i^{NPFC} is usually called the network power frequency characteristic. It can be used to assess the "area control error"

$$E_i = P_i^{dc} - \bar{P}_i^{dc} + \lambda_i^{\text{NPFC}}\,(f_i - f_{nom,i})\,, \tag{41}$$

which differs from 0 in steady-state only if there is a power imbalance directly in area i itself. This allows the secondary frequency controller of each individual area i to efficiently detect power imbalances that originate from its particular area i, despite the network coupling through the HVDC grid.

Secondary frequency control should increase P_{mi}^o if E_i is negative, since by definition (38) this means that $(P_{mi}^o - P_{li}^o)$ must have decreased with respect to its expected value. In practice, this can be implemented by an integral controller that modifies P_{mi}^o according to

$$P_{mi}^o = \bar{P}_{mi}^o - \beta_i \int E_i dt\,, \tag{42}$$

where $\beta_i > 0$ is the secondary frequency controller gain of area i. The value of β_i should be chosen small enough so that P_{mi}^o can be considered constant on the time scale of primary frequency control.

6.2 Simulation results

To illustrate the impact of secondary frequency control, we run simulations under the same conditions as in Section 5. Figures 5 and 6 depict the evolution of the frequencies and the power setting P_m^o of the five AC areas when the primary and the secondary frequency control schemes proposed in the present paper are implemented. As secondary frequency control has a time scale of a few minutes, we extend the observation window to 5 minutes. The controller gains are chosen as $\beta_1 = \ldots = \beta_5 = 10$.

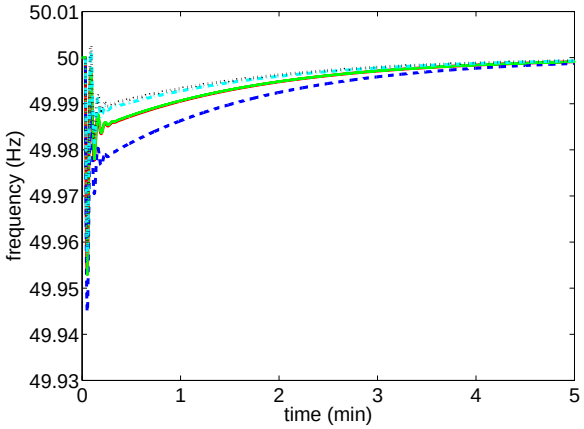

Figure 5: Frequencies of the five AC areas when secondary frequency control is used in combination with our primary frequency control scheme.

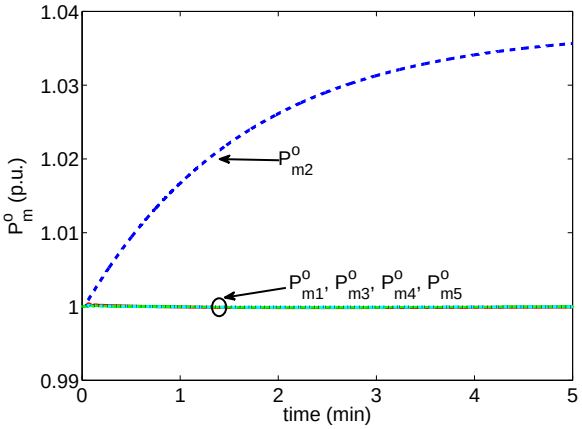

Figure 6: P_m^o of the five AC areas when secondary frequency control is used in combination with our primary frequency control scheme.

The behavior during the first few seconds on Figure 5 is essentially equal to Figure 3. This means that the primary frequency control dominates, unperturbed by secondary frequency control. The latter also performs as expected: only the power setting for the disturbed area 2, P_{m2}^o, is changed significantly, and the frequencies converge back to their nominal values in the long term. The evolution of the P_i^{dc} indicates that the power injections into the DC grid are also restored to their nominal values (the graphs are not shown due to space constraints).

7 Conclusions

In this paper, we present a decentralized control scheme to share primary frequency reserves among non-synchronous AC areas connected by a multi-terminal HVDC system. With this control scheme, the converters modify their DC-side voltages so that the frequency deviations evolve in a similar manner. Theoretical study of a simplified case supports that the interconnected system is stable and converges to an equilibrium at which, for bounded load perturbations, the differences between the frequency deviations induced in all the areas can be made arbitrarily small by choosing a sufficiently large control gain. Simulations run on a benchmark system with five non-identical areas show that the frequency deviations are always reduced by our reserve-sharing primary frequency controller. The simulations also highlight that the control scheme can successfully be combined with secondary frequency control.

This work suggests several research directions. First, the theoretical study could be extended by relaxing some of the assumptions done for establishing the proofs. In particular, we would like to extend our theoretical results to the case where the AC areas have different parameters. Second, it would be interesting to study the properties of the scheme when the individual areas have different sub-controller gains. Indeed, these gains influence the degree of participation of every area in the primary frequency control scheme, and, by better understanding their influence, one should be able to choose them so as to take into account the technical and economic characteristics of each

area. These gains could probably also be tuned dynamically in the time frame of the secondary frequency control scheme, so as to reflect the change of the operating point and reduce the likelihood of congestions in the DC lines following a disturbance. Third, while the primary frequency control scheme proposed in this paper calls for primary frequency reserves simultaneously from all areas of the system in the aftermath of a power imbalance in an area, we believe that it would also be worth investigating whether it could be adapted to the case where the primary frequency reserves of different areas are solicited in a sequential way, so that the reserves from remote areas are deployed only when local reserves have been depleted.

Finally, using a multi-terminal HVDC grid for sharing primary frequency reserves between the AC areas may have an adverse effect. Indeed, the areas may become more vulnerable with respect to contingencies resulting in a disconnection from the HVDC link, because such contingencies may create a dangerous power imbalance in an area while at the same time reducing the primary frequency reserves that the area has access to. This is certainly an issue to be considered when relying on an HVDC system for offering such a type of ancillary service.

Acknowledgment

The authors are grateful to Raphaël Fonteneau and Alexandre Mauroy, both from the University of Liège, for their valuable comments on the proof of Proposition 3. They also thank Patrick Panciatici from RTE (French TSO) for pointing out the need of studying the control scheme when combined with secondary frequency control.

Alain Sarlette is a FRS-FNRS postdoctoral research fellow and Damien Ernst is a FRS-FNRS research fellow. They thank the FRS-FNRS for its financial support. This paper presents research results of the Belgian Network DYSCO (Dynamical Systems, Control, and Optimization), funded by the Interuniversity Attraction Poles Programme, initiated by the Belgian State, Science Policy Office. The scientific responsibility rests with its authors.

REFERENCES

[1] P. de Toledo, J. Pan, K. Srivastava, W. Wang, and C. Hong, "Case study of a multi-infeed HVDC system," in *Proceedings of Joint International Conference on Power System Technology and IEEE Power India Conference, 2008. POWERCON 2008*, pp. 1–7, October 2008.

[2] G. Fujita, G. Shirai, and R. Yokoyama, "Automatic generation control for DC-link power system," in *Proceedings of IEEE/PES Transmission and Distribution Conference and Exhibition 2002: Asia Pacific*, vol. 3, pp. 1584–1588, October 2002.

[3] J. Dai, Y. Phulpin, A. Sarlette, and D. Ernst, "Coordinated primary frequency control among non-synchronous systems connected by a multi-terminal HVDC grid," Submitted.

[4] UCTE, "UCTE operation handbook, v 2.5." [Online]. Available: http://www.ucte.org, 2004.

[5] J. Dai, Y. Phulpin, A. Sarlette, and D. Ernst, "Impact of delays on a consensus-based primary frequency control scheme for AC systems connected by a multi-terminal HVDC grid," in *Proceedings of Bulk Power System Dynamics and Control (iREP) - VIII (iREP), 2010 iREP Symposium*, pp. 1–9, August 2010.

[6] P. Kundur, *Power System Stability and Control*. New York: McGraw-Hill, 1994.

[7] L. L. Grigsby, *Power System Stability And Control*. Electrical Engineering Handbook Series, Boca Raton: CRC Press Inc., 2007.

[8] M. L. Ourari, L.-A. Dessaint, and V. Q. Do, "Generating units aggregation for dynamic equivalent of large power systems," in *Proceedings of IEEE Power Engineering Society General Meeting*, vol. 2, pp. 1535–1541, June 2004.

[9] B. H. . Bakken and H. H. Faanes, "Technical and economic aspects of using a long submarine HVDC connection for frequency control," *IEEE Transactions on Power Systems*, vol. 12, pp. 1252–1258, August 1997.